Dendrites are dispensable for basic motoneuron function but essential for fine tuning of behavior

Stefanie Ryglewski[1], Dimitrios Kadas[1], Katie Hutchinson, Natalie Schuetzler, Fernando Vonhoff[2], and Carsten Duch[3]

Institute of Neurobiology, Johannes Gutenberg University of Mainz, 55099 Mainz, Germany

Edited by John G. Hildebrand, University of Arizona, Tucson, AZ, and approved October 27, 2014 (received for review August 22, 2014)

Dendrites are highly complex 3D structures that define neuronal morphology and connectivity and are the predominant sites for synaptic input. Defects in dendritic structure are highly consistent correlates of brain diseases. However, the precise consequences of dendritic structure defects for neuronal function and behavioral performance remain unknown. Here we probe dendritic function by using genetic tools to selectively abolish dendrites in identified *Drosophila* wing motoneurons without affecting other neuronal properties. We find that these motoneuron dendrites are unexpectedly dispensable for synaptic targeting, qualitatively normal neuronal activity patterns during behavior, and basic behavioral performance. However, significant performance deficits in sophisticated motor behaviors, such as flight altitude control and switching between discrete courtship song elements, scale with the degree of dendritic defect. To our knowledge, our observations provide the first direct evidence that complex dendrite architecture is critically required for fine-tuning and adaptability within robust, evolutionarily constrained behavioral programs that are vital for mating success and survival. We speculate that the observed scaling of performance deficits with the degree of structural defect is consistent with gradual increases in intellectual disability during continuously advancing structural deficiencies in progressive neurological disorders.

dendrite | synapse | motor behavior | courtship | *Drosophila*

Dendrites are structural ramifications of a neuron specialized for receiving and processing synaptic input (1). The estimated 100 billion neurons in the human brain (2) form approximately 100 trillion synapses onto a total of approximately 100,000 miles of dendritic cable. The functions of dendrites are proposed to range from simply providing enough surface for synaptic input (3) to highly compartmentalized units of molecular signaling and information processing (4–6). In addition to functioning as passive receivers, dendrites may be equipped with output synapses (7) and active membrane currents (8), which add tremendous computational power to a single neuron (6, 9, 10).

Accordingly, dendritic abnormalities are highly consistent anatomical correlates of numerous brain disorders (11, 12), including autism spectrum disorders, Alzheimer's disease, schizophrenia, Down syndrome, Fragile X syndrome, Rett syndrome, anxiety, and depression. However, in many cases it remains unclear whether dendritic defects are the cause or the consequence of impaired brain function. Trying to understand dendrite function poses major technical challenges because it requires selective manipulation of dendritic structure without disturbing other properties of the affected neuron, followed by quantitative analysis of neuronal function and the resulting behavioral consequences.

This study uses the *Drosophila* genetic model system to selectively abolish dendrites from a subset of identified wing muscle motoneurons that have well-described and stereotyped dendritic morphologies (13) and firing patterns during flight (14) and courtship song (15, 16). Surprisingly, we find that motoneurons that lack 90% of their dendrites are still contacted by appropriate synaptic partners and produce qualitatively normal firing patterns and wing movements during flight and courtship song. However, normal dendritic architecture is essential for particularly challenging tasks, such as the integration of optomotor input for adequate control of flight power output, or the temporal accuracy of switching between different song elements during courtship to ensure mating success. Our data demonstrate that the vast majority of basic motor functions can be satisfactorily accomplished with motoneurons that have significant dendritic defects but normal axonal structure and membrane currents. However, a complex 3D dendritic architecture is mandatory for intricate regulation of behavioral output, which in turn imposes a positive selection pressure on the maintenance of such complex dendritic trees through evolution.

Results and Discussion

Drosophila wing movements during flight and the male courtship song are powered by stretch-activated, asynchronous flight muscles. Wing depression is mediated by the dorsal longitudinal flight muscle (DLM), consisting of six muscle fibers, which are innervated by five motoneurons, MN1–5 (Fig. 1*A*) (17), for which firing patterns and function are well known and can be recorded in vivo during restrained flight (14, 18). We have described the dendritic structure (19–21) and membrane properties (19, 22, 23) of one such neuron, MN5, in particular detail. MN5 is a unipolar neuron with its soma contralateral to the DLM target muscle (Fig. 1 *A* and *B*). All dendrites branch off a primary neurite that merges into the axon further distally (Fig. 1*B*). MN5 can be unambiguously identified from animal to animal and displays a stereotyped dendritic morphology comprising a total length of 6,500 μm and >4,000 branches (13). Dendritic architecture is tightly regulated during development by steroid hormones (24), calcium signaling (25), neural activity (19, 20), and cell surface signals (26). We have previously shown that the

Significance

Approximately 100 billion neurons in our brain form 100 trillion synapses onto 100,000 miles of dendritic cable. Accordingly, dendritic defects are consistent anatomical correlates of numerous brain diseases, but specific causality remains unproven. Here we genetically remove dendrites in *Drosophila* motoneurons, followed by analysis of functional outcomes. We find that dendrites are surprisingly dispensable for basic nervous system function and simple behavioral tasks. By contrast, highly complex dendritic architecture is required for adaptive refinement of sophisticated motor tasks that are vital for survival and reproduction. Here the degree of dendritic defect scales with the degree of performance deficit. We postulate that during evolution the maintenance of complex dendritic structure is under high selective pressure.

Author contributions: S.R. and C.D. designed research; S.R., D.K., K.H., N.S., F.V., and C.D. performed research; C.D. contributed new reagents/analytic tools; S.R., D.K., K.H., N.S., F.V., and C.D. analyzed data; and S.R. and C.D. wrote the paper.

The authors declare no conflict of interest.

This article is a PNAS Direct Submission.

[1]S.R. and D.K. contributed equally to this work.

[2]Present address: Department of Molecular, Cellular, and Developmental Biology, Yale University, New Haven, CT 06520.

[3]To whom correspondence should be addressed. Email: cduch@uni-mainz.de.

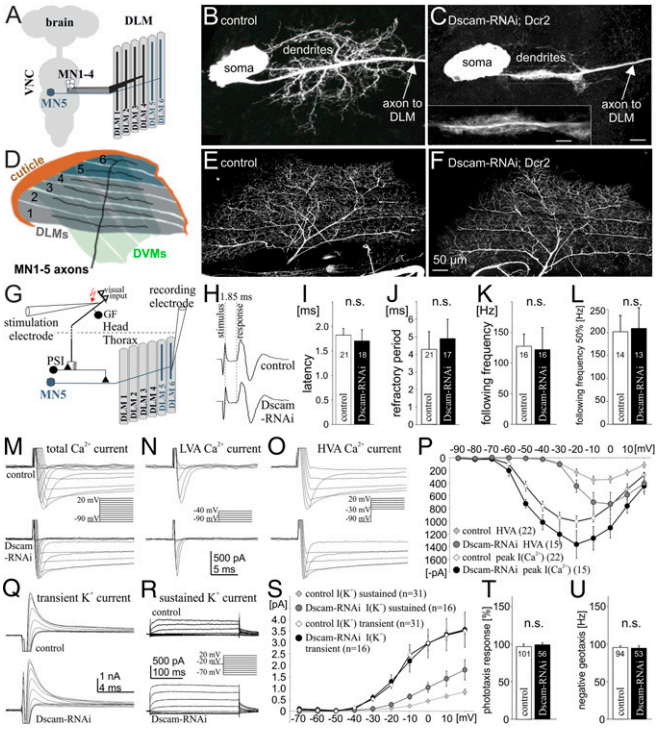

Fig. 1. Selective manipulation of dendrites. (*A*) Schematic of *Drosophila* dorsal longitudinal wing depressor muscle and its innervation by motoneurons, MN1–5. (*B*) Representative image of MN5 dendritic structure in a control. (*C*) MN5 structure after targeted RNAi knockdown of Dscam1. (*D*) Schematic of DLM fibers with MN1–5 axon arbors. (*E* and *F*) MN1–5 axonal projections and collateral branches are similar in controls (*E*) and after dendrite elimination (*F*). (*G*) Schematic of the *Drosophila* neuronal escape circuit. Visual input is relayed to the GF interneuron that makes a mixed electrical chemical synapse onto the PSI, which in turn bypasses all dendrites and synapses onto the axons of MN1–5. (*H*) Postsynaptic responses in the DLM muscle after GF stimulation are identical in controls and after genetic elimination of most motoneuron dendrites, indicating normal speed of action potential propagation and synaptic transmission. (*I–L*) Reliability of synaptic transmission is not affected by dendritic defects. Refractory period remains unaltered (*J*); the pathway follows stimulation frequencies of approximately 130 Hz with 100% reliability (*K*) and up to 200 Hz with 50% reliability (*L*). (*M*) MN5 voltage-gated Ca^{2+} currents are qualitatively similar in controls and with 90% dendrite reduction, both with respect to low-voltage activated (LVA) (*N*) and high-voltage activated (HVA) currents (*O*). (*P*) Activation voltages of LVA and HVA currents are identical in controls ($n = 22$) and manipulated neurons (n =15), but current amplitudes as recorded from the soma are larger in neurons with significantly reduced dendrites. (*Q* and *R*) A-type (*Q*) and sustained (*R*) K^+ currents are qualitatively similar in controls and MN5 with dendritic defects. (*S*) Activation voltages of transient and sustained K^+ currents are not affected by Dscam1 RNAi. Transient K^+ current is identical to controls ($n = 31$), but sustained K^+ current displays a larger amplitude in MN5 with defective dendrites ($n = 16$). (*T*) Positive phototaxis and negative geotaxis responses (*U*) are normal after targeted expression of Dscam1 RNAi under the control of C380-GAL4;; Cha-GAL80.

Down syndrome cell adhesion molecule 1, Dscam1, is required cell-intrinsically for normal dendrite formation during development (26). Targeted RNAi knock down of Dscam1 in MN1–5 (*Experimental Procedures*) always causes one of two distinctly different dendritic defects. In 60% of all preparations it abolishes more than 90% of all dendrites and leaves the primary neurite decorated with lamellipodia-like structures (Fig. 1*C*) (26). In the remaining 40% of all preparations it reduces dendritic length and branching to 50% of controls (26) (see Fig. 3*B*). In this study we have determined the degree of dendritic defects in each experiment by intracellular dye filling.

Selective Manipulation of Neuronal Dendrites. In the first set of experiments we show that 90% of all wing depressor motoneuron dendrites can be selectively abolished by targeted Dscam1 RNAi knock down without affecting other properties of these neurons. The axon terminals of MN1–5 branch in a stereotyped fashion over the DLM target muscle, with MN1–4 innervating the four ventral-most fibers and MN5 innervating DLM fibers 5 and 6 (Fig. 1*D*). Innervation of all six DLM fibers by MN1–5, and axon collateral sprouting are similar in controls (Fig. 1*E*, $n = 8$) and after 90% dendrite elimination via Dscam1 knockdown (Fig. 1*F*, $n = 8$). To test for potential defects in action potential propagation or neuromuscular transmission, we used the well-described escape response circuit of *Drosophila* (27). In this circuit visual information is transmitted to the giant fiber interneuron that synapses onto the peripherally synapsing interneuron (PSI) in the thoracic ganglion, which in turn synapses directly onto the axon of MN5, thus bypassing all dendrites (Fig. 1*G*). Electrical stimulation of the giant fiber interneuron reliably elicits action potentials in the axon of MN5, which in turn are transmitted to the DLM target muscle. In this fast escape circuit the delay between giant fiber stimulation and muscle potential is 1.85 ± 0.21 ms (Fig. 1*H*) and remains unaltered in motoneurons with significant dendritic defects (Fig. 1 *H* and *I*). Therefore, the speed of action potential propagation, synaptic transmission from PSI to the motoneuron axon, and neuromuscular transmission remain normal. Similarly, reliability of signal transmission through this circuit is not altered after 90% dendrite removal in motoneurons: refractory period (Fig. 1*J*) and muscle following frequency at high-frequency stimulation remain as in controls (Fig. 1 *K* and *L*).

Furthermore, even with severe dendritic defects, MN5 ionic currents remain qualitatively normal. In controls, and after elimination of 90% of all dendrites, MN5 displays low- (Fig. 1 *M* and *N*) and high-voltage activated calcium currents (Fig. 1 *M* and *O*; note that the dendritic phenotypes were confirmed in each voltage clamp experiment by dye filling). Current amplitudes of both calcium currents as recorded from the soma are larger after Dscam1 knockdown-induced dendritic defects compared with controls (Fig. 1*P*). This is expected, because MN5 displays dendritic calcium currents that are partially hidden to somatic voltage clamp recordings by space clamp limitations in control neurons (23). Similarly, sustained outward potassium currents are qualitatively normal in MN5 with Dscam1 RNAi-induced dendritic defects (Fig. 1*R*). Again, current amplitude as recorded from the soma is larger in neurons with dendritic defects (Fig. 1*S*). By contrast, the transient A type-like potassium current is qualitatively and quantitatively normal in MN5 with severe dendritic defects (Fig. 1 *Q* and *S*). Axonal currents are expected to display normal amplitudes in neurons with dendritic defects, and transient Shaker A-type potassium channels are localized to the axon of MN5 (22). Therefore, all currents measured are qualitatively identical to controls after Dscam1 knockdown. Ionic currents mediated by channels with predicted dendritic localization are of larger amplitude in motoneurons with reduced dendrites, as expected with increased space clamp control in smaller neurons with less-complex dendrites.

Although Dscam1 is required cell autonomously for flight motoneuron dendritic growth (26), our GAL4 expression system (see *Methods*) also causes some RNAi expression in nonidentified neurons in the brain. Therefore, we conducted additional behavioral tests to control for possible nonspecific effects of our manipulation in other brain regions. Animals displayed normal positive phototaxis (Fig. 1*T*), as well as negative geotaxis responses (Fig. 1*U*), including normal climbing speeds.

In summary, targeted Dscam1 RNAi knockdown in wing MN1–5 selectively eliminates dendrites without affecting axonal branching, neuromuscular transmission, action potential propagation, synaptic transmission onto motoneuron axons, or ion

channel expression, thus allowing us to specifically probe the roles of dendritic arborization for motoneuron function.

Flight Without Wing Depressor Motoneuron Dendrites. We used a tethered flight assay (28) to test motor performance in animals with defective dendrites in wing depressor motoneurons (Fig. 2*A*). To our surprise no obvious flight defects were observed. Even animals with a 90% reduction of depressor motoneuron dendrites were able to fly, although they show slightly but significantly reduced flight durations in this assay (Fig. 2*B*). Flight and dendritic phenotypes were directly correlated in our experiments: defects in dendrite branching were confirmed by intracellular dye fills after each behavioral experiment. Flight initiation likelihood as measured by the number of subsequent flight bouts that can be induced by wind stimuli to the head (Fig. 2*C*) and the mean flight bout duration (Fig. 2*D*) were not altered significantly.

Nearly normal tethered flight patterns in manipulated animals indicate that depressor motoneurons with severe dendritic structure defects might still receive synaptic input from the central pattern-generating network. To directly visualize potential synaptic inputs to motoneurons with defective dendrites, we next tested whether presynaptic markers would localize to the lamellipodia-like structures that decorate the MN5 primary neurite after Dscam1 RNAi-induced dendrite elimination (Fig. 2*E*). As a presynaptic marker, we use immunolabeling against the active zone protein Bruchpilot, Brp (29). Single optical sections reveal that many labeled active zones of unidentified presynaptic terminals localize precisely to the edges of these lamellipodia-like structures on the motoneuron primary neurite (Fig. 2*E*). By contrast, the primary neurite and the neuropil region just outside these structures are devoid of Brp-positive label. Colocalization analysis of single optical sections from eight preparations revealed a fivefold higher pixel density for Brp-positive pixels colabeled with MN5 lamellipodia-like structures compared with neuropil regions within 1-μm distance, indicating that presynaptic neurons target lamellipodia-like structures in motoneurons with defective dendrites. However, confocal microscopy does not provide sufficient spatial resolution to unambiguously identify synaptic inputs in situ. Therefore, additional physiological experiments were conducted. Normally MN5 receives excitatory drive via the Dα7 nicotinic ACh receptor and inhibitory GABAergic input via the Rdl $GABA_A$ receptor (21, 30). Picospritzing the cholinergic agonist nicotine into the flight neuropil reliably evokes postsynaptic potentials as recorded from the motoneuron somata, both in controls (Fig. 2*F*, $n = 14$) and in manipulated motoneurons that lack more than 90% of their dendrites (Fig. 2*G*, $n = 14$). Somatic postsynaptic potentials (PSPs) were slightly sharper and of larger amplitude compared with controls (Fig. 2 *H* and *I*), as expected with signal attenuation and broadening being larger in neurons with complex dendrites, where synaptic sites are more distant from the recording location. Similarly, picospritzing GABA into the flight motor neuropil evokes hyperpolarizing postsynaptic potentials in MN5, both in controls (Fig. 2*J*, $n = 12$) and with 90% dendrite reduction (Fig. 2*K*, $n = 12$). Without dendrites somatic inhibitory postsynaptic potentials (IPSPs) were of larger amplitude compared with controls (Fig. 2 *L* and *M*), likely owing to reduced signal attenuation. Finally, action potentials can be evoked by injections of nicotine into the flight neuropil in controls and in manipulated animals (Fig. 2 *N* and *O*). Together, these data indicate that wing motoneurons that lack more than 90% of all dendrites still receive enough inhibitory and excitatory synaptic inputs to evoke normal action potentials. Note that lamellipodia-like structures that remain in motoneurons with 90% dendrite loss never cover the normal dendritic territory of these motoneurons (Fig. 1 *A* and *C*), meaning that potential presynaptic partners must adjust their growth patterns to reach postsynaptic motoneurons. These observations are comparable to mouse retina, where DSCAMs are required for normal neuron spacing and dendrite development but are not essential for synaptic specificity (31).

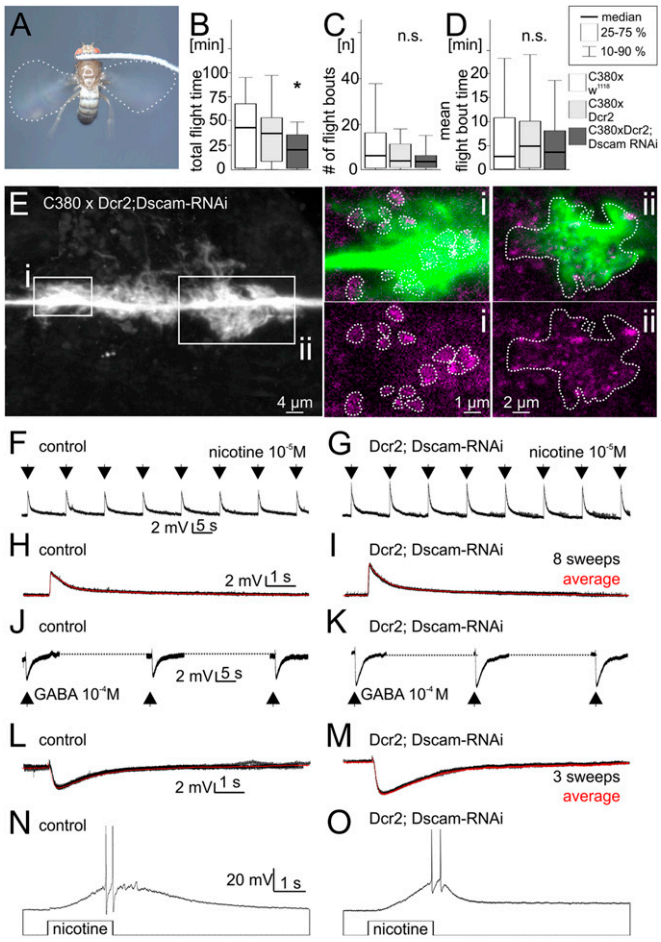

Fig. 2. Dendrites are dispensable for synaptic input to wing motoneurons, and manipulated animals can fly. (*A*) Flies with Dscam1 RNAi-induced dendritic defects in wing motoneurons readily engage in tethered flight. (*B–D*) Significant dendritic defects cause only mild flight behavioral deficits. (*B*) Total flight duration is decreased in animals with wing motoneuron dendritic defects (dark gray bar) compared with control (white and light gray bars). (*C* and *D*) Both the number of flight initiations upon wind stimuli to the head (*C*) and the mean duration of individual flight bouts (*D*) are not reduced significantly. (*E*) In MN5 with defective dendrites lamellipodia-like structures that decorate the primary neurite are in direct proximity to immunolabeled presynaptic active zones of other neurons. White boxes show regions for which selective enlargements of single optical sections are shown (i, ii, lamellipodia-like structures in green, active zones in magenta). Dotted white lines in i encircle active zone. Dotted white lines in ii depict outline of lamellilpodia. (*F–I*) Picoinjection of nicotine (10^{-5} M in saline, 3-ms injection duration) into MN5 lamellipodia regions reliably evokes postsynaptic potentials as recorded from the soma both in controls (*F*) and without any normal dendrites (*G*). Recordings are performed in 10^{-7} M TTX to exclude possible indirect effects via excitation of other neurons. (*H* and *I*) Overlays of eight sweeps (black traces) and average postsynaptic responses (red traces) display larger amplitudes in manipulated animals than in controls, because signal attenuation to the somatic recording site is reduced. (*J–M*) Picoinjections of GABA (10^{-4} M in saline, 3-ms injection duration) show that MN5 lamellipodia express $GABA_A$ receptors in controls (*J* and *L*) and after Dscam1 RNAi-induced dendritic defects (*K* and *M*). (*N* and *O*) Longer-duration injections (2 s) of nicotine in the absence of TTX reliably evoke action potentials in controls (*N*) and after dendrite elimination (*O*), demonstrating that even in the absence of all normal dendrites strong cholinergic excitation is sufficient to drive motoneuron firing.

Dendrites and Flight Altitude Control. *Drosophila* flight is powered by asynchronous muscles, so that wing power muscle contractions are not synchronized with motoneuron action potentials (32).

Instead, alternating elevator and depressor muscle contractions are initiated at approximately 200 Hz frequency by antagonistic stretch activation, and wing motoneurons fire tonically at frequencies of 4–20 Hz to fuel the muscle with intracellular calcium (33). Adjustments of intramuscular calcium and power output are generated by changes in tonic motoneuron firing frequencies (34). Therefore, wing depressor motoneurons fuel the flight motor but are not critical for wing beat coordination. However, genetic ablation of wing depressor motoneurons ($n = 12$) or silencing by inwardly rectifying K_{ir} channel expression completely abolish the animals' ability to fly ($n = 8$), demonstrating that asynchronous flight requires depressor motoneuron activity. To test whether synaptic drive from the central motor networks elicits normal firing patterns in these motoneurons during flight, we next recorded MN5 firing patterns with fine tungsten wires from its target muscle fiber in vivo during tethered flight. Each extracellular muscle fiber potential corresponds to one MN5 action potential. These experiments are designed to correlate different degrees of dendritic defects to motoneuron performance. As stated above, Dscam1 RNAi knockdown can induce either a reduction of wing depressor motoneuron dendrites by approximately 50% (Fig. 3*B*) or by more than 90% (Fig. 3*C*) (26). In each animal tested, MN5 was first recorded in vivo during tethered flight and then filled intracellularly to determine the degree of dendritic defect. Independent of the severity of the dendritic phenotype, flight can be initiated by a wind stimulus to the head, and MN5 fires tonically throughout the duration of the flight bout (Fig. 3 *E*–*G*). However, reductions of MN5 dendritic length scale with decreases in firing frequency (Fig. 3 *D*–*G*) and spike time precision (Fig. 3*H*). The most parsimonious explanation is that more dendritic cable allows for more synaptic input, and the more synaptic input the motoneurons receive, the higher are the resulting firing frequency and temporal precision within bouts of tonic firing. Nevertheless, even with reductions in wing depressor motoneuron dendrite cable by more than 90%, animals are able to fly relatively normally.

Because animals do not have to support their own weight in tethered flight, we next tested whether normal dendritic architecture is needed for more challenging flight tasks. We presented the animals with vertical oscillations of a horizontal stripe pattern (Fig. 3*L*). As reported previously (34), control flies increase motoneuron firing frequencies, and thus thrust and lift, in response to rising stripes, which deceive the animal into the illusion of losing altitude. Conversely, decreased motoneuron firing frequencies are observed in response to falling stripes (Fig. 3 *I* and *M*). This translation of optomotor input into adaptive changes of motoneuron firing frequencies is still observed in animals with moderate dendritic defects (Fig. 3 *J* and *N*; 50% reduction) and to some degree even with severe dendritic defects (Fig. 3 *K* and *O*). However, the larger the dendritic architecture defect, the lower the impact of optomotor input on changes in motoneuron firing frequency, and the longer it takes to modulate motoneuron firing frequency (Fig. 3*P*). Therefore, the ability to adequately adjust flight muscle power input to the illusion of flight altitude changes decreases with increased severity of motoneuron dendritic structure defects.

In summary, at least for basic performance, complex dendritic structure seems surprisingly dispensable. Despite quantitative decreases in response amplitude and speed, motoneuron responses to optomotor input are qualitatively normal even without any normally branched dendrites (Fig. 3 *K*, *O*, and *P*).

Dendrites Are Needed for Successful Love Song. Wing depressor motoneurons are also needed to power wing downstroke during male courtship song, a motor behavior that is required to attract females during the *Drosophila* mating ritual (16). During this behavior the male orients toward the female, spreads out one wing (Fig. 4*A*), and produces a species-specific sound pattern that consists of two elements. First, low amplitude up and down movements of the wing of approximately 160-Hz frequency (sine song), and second, bouts of large-amplitude wing strokes that occur with a species-specific interpulse interval (IPI) that lasts approximately 34 ms in *Drosophila melanogaster* (pulse song). Both sine and pulse song can be recorded with a microphone and are qualitatively identical in control flies (Fig. 4*B*), flies with a 50% reduction in wing depressor motoneuron dendrites (Fig. 4*C*), and flies that lack more than 90% of all wing motoneuron dendrites (Fig. 4*D*). However, although male flies with defective wing depressor motoneuron dendrites can produce orderly sine and pulse song elements (Fig. 4 *B*–*D*), their mating success

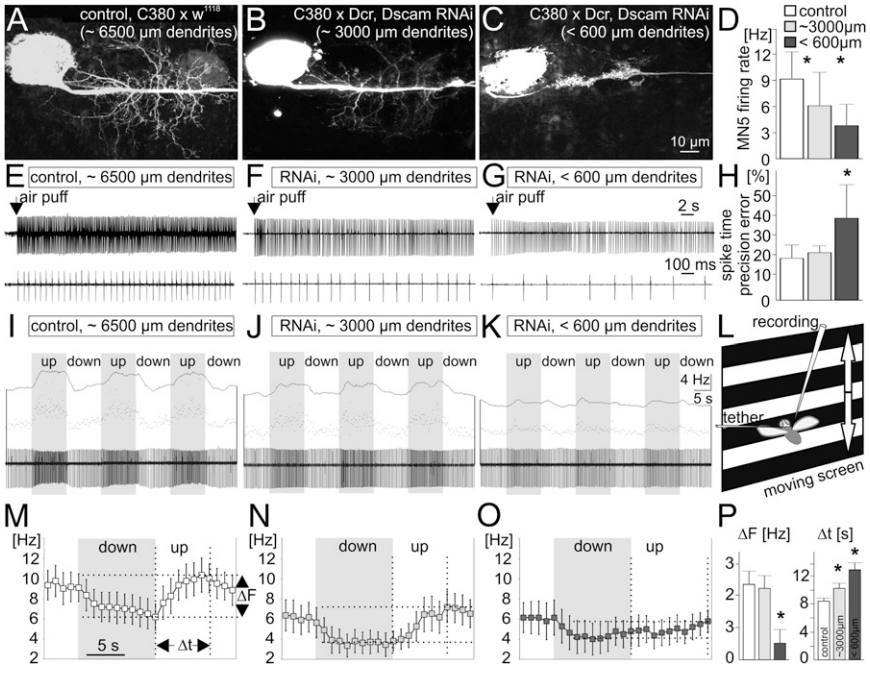

Fig. 3. Dendritic defects scale with specific flight defects. (*A*–*C*) Compared with controls (*A*), Dscam1 RNAi reduces MN5 dendrites either by approximately 50% (*B*) or by 90% (*C*). (*D*–*H*) Independent of the dendritic defect, MN5 fires tonically during tethered flight (*E*, control; *F*, 50% dendrite reduction; *G*, 90% dendrite reduction). Dendritic defect severity scales with decreases in average firing frequencies (*D*), as do deviations from a constant interspike interval (*H*). (*I*–*P*) Spike frequency modulations in response to optomotor input scale down significantly with the severity of dendritic defects. (*L*) Presenting vertically moving stripes simulates rising (downward stripes) or decreasing (upward stripes) flight altitude, resulting in MN5 firing frequency modulations in control flies (*I*). These also occur with a 50% dendrite reduction (*J*) but are strongly reduced with 90% dendrites absent (*K*). (*M*–*O*) Mean firing frequency modulations (eight animals per group) during downs (gray) and ups (white); *M*, control; *N*, 50% dendrite reduction; *O*, 90% dendrite reduction. ΔF signifies maximum frequency modulations and Δt the durations between minimum and maximum frequencies. (*P*) ΔF is significantly reduced only with a reduction in dendrites by more than 90%. Δt scales significantly with the dendritic defect severity (ANOVA, Newman Keuls post hoc test, $P \leq 0.05$).

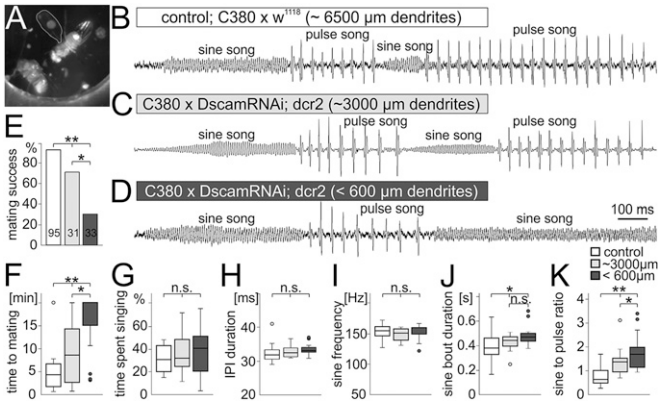

Fig. 4. Song quality and mating success scale with the severity of dendritic defects. (*A–C*) During courtship song the male fly orients toward the female, spreads out one wing (*A*), and produces two distinctly different song elements by up and down wing movements. (*B*) Sound patterns with low amplitude and an average frequency of 155 ± 10 Hz are named sine song, whereas high-amplitude sound pulses with an average IPI of 33 ± 3 ms are named pulse song. (*C*) Animals with a 50% reduction in wing depressor motoneuron dendrites produce normal sine and pulse song elements. (*D*) Even with 90% dendrite reduction sine and pulse song frequencies and amplitudes are similar to controls. (*E*) However, mating success within 20 min decreases from 96% in controls (white), over 64% with 50% dendrite reduction (light gray) to 21% with 90% dendrite reduction (dark gray). Thus, mating failure rates scale with the dendritic defect severity. (*F*) Similarly, the time to mating increases significantly with the dendritic defect severity. (*G*) However, all three groups spend the same amounts of time singing. (*H* and *I*) IPI (*H*) and sine song frequency (*I*) are statistically identical in all groups. (*J*) The average sine bout duration is significantly increased in animals with Dscam1 RNAi expression. (*K*) Summing up all sine and pulse song bouts reveals a statistically significant increase of the sine to pulse song ratio with 50% dendrite reduction compared with controls. In animals with 90% reduction of wing motoneuron dendrites the sine to pulse song ratio is significantly further increased (Kruskal Wallis ANOVA with post hoc *U* tests).

within 20 min decreases significantly and scales with the severity of the dendritic phenotype, with 96% success in controls, 64% success with 50% dendritic length reduction, and 21% success with 90% dendritic length reduction (Fig. 4*E*). If males with genetically abolished wing motoneuron dendrites are successful in mating they require significantly more time to attract the female, and this duration again scales with the severity of the dendritic phenotype (Fig. 4*F*). This reduction in mating success is not caused by less song production: all test groups spend similar periods of time singing once presented with a female (Fig. 4*G*). Additionally, the structure within each of both song elements, pulse song (Fig. 4*H*) and sine song (Fig. 4*I*), is identical with or without wing motoneuron dendrites. This is consistent with recent findings that motoneurons to direct wing muscles, other than the wing depressor motoneurons, are required for the initiation of either sine or pulse songs (35). However, wing depressor motoneurons are recruited at low frequencies during sine song elements and switch to higher firing frequencies during pulse song (15) to fuel the wing power muscle. Dendritic defects in wing depressor motoneurons (Fig. 4 *B–D*) cause increases in the duration of sine song elements (Fig. 4*J*), which scale with the severity of the dendritic defect. This in turn reverses the sine-to-pulse song ratio (Fig. 4*K*). Controls with 96% mating success sang approximately 40% sine song and 60% pulse song, whereas animals with moderate dendritic defects in wing depressor motoneurons sang approximately 55% sine song and showed 64% mating success. Severe dendritic defects resulted in 70% sine song and less than 25% mating success. Wild-type flies dynamically modulate song structure, including sine to pulse song ratios, in response to different sensory experience during the mating ritual (36). We show that complex dendritic architecture in wing depressor motoneurons is required to adequately perform such adjustments and ensure mating success. Reduced dendritic surface impairs the ability to quickly modulate motoneuron firing frequency as needed for switching from sine to pulse song (15). This is consistent with the decreased ability to rapidly modulate firing frequency in response to optomotor input for altitude control during flight (Fig. 3 *I–P*).

In conclusion, our data demonstrate that complex dendritic architecture is dispensable for synaptic partner matching, because motoneurons with abnormal dendrites receive synaptic input that suffices to produce qualitatively normal firing patterns during behavior. This is consistent with recent findings in mouse retina whereby DSCAM is required for normal structural organization but not for appropriate synaptic wiring (31). A possible explanation is that cues for synaptic partner recognition are set by neuronal identity, and presynaptic contacts end up elsewhere in the neuronal membrane if dendrites are absent. However, significant decreases in dendritic length strongly reduce the surface available for synaptic input. In larval *Drosophila* motoneurons developmental arrest of dendrite growth correlates with decreased synaptic input (37). Accordingly, we found that impairments in adjusting neuronal firing frequency and motor performance scale with the amount of reduced dendritic surface. We speculate that a similar relationship underlies gradual increases in intellectual disability during mammalian/human development and during continuously advancing structural deficiencies in progressive neurological disorders (12, 38). Scaling of firing frequency and spike time scatter with the degree of dendritic defect are in accordance with the hypothesis that wing power motoneurons translate the integrated amount of tonic excitation into tonic firing frequencies, as was previously proposed (14). At least for this operational mode of wing depressor motoneurons, basic function is qualitatively normal even with severe dendritic defects. Similarly, basic network dynamics is often recapitulated in models without morphology (39). However, our data demonstrate a high positive selection pressure on expensive dendritic architectures with more than 6 mm of total length even for neurons that do not rely on high spike time precision or other delicate dendritic computation. Evolutionarily important functions, such as appropriate flight power output control and high mating success, require the full complexity of the dendritic arbor.

Experimental Procedures

Animals. *Drosophila melanogaster* were reared in 68-mL vials on a standard yeast corn meal medium at 25 °C, with a 12-h light/dark regimen and 60% humidity (19). Flies were used 1–2 d after eclosion (for courtship 2 d after eclosion). We used the binary GAL4/UAS expression system to express transgenes (40). As previously described (20), C380-GAL4, UAS-mCD8::GFP;; Cha-GAL80 was used to restrict transgene expression to a subset of wing depressor motoneurons and some additional unidentified neurons. The Cha-GAL80 transgene inhibited expression in unidentified cholinergic interneurons, leaving expression in approximately 30 neurons per segment in the ventral nerve cord (41). To knock down Dscam1, male UAS-Dscam RNAi transgenic flies (VDRC, Vienna *Drosophila* RNAi Center, 36233) were crossed to female C380-GAL4, UAS-mCD8::GFP;; Cha-GAL80 flies. We have previously shown (26) that two additional different UAS-Dscam RNAi transgenes yielded similar results (VDRC, fly stock numbers 108835 and 25623). In all experiments UAS-Dcr2 (Bloomington 24650) was coexpressed with UAS-Dscam1 RNAi to enhance transgenic RNAi effects (42) as reported previously (26). As controls, C380-GAL4, UAS-mCD8::GFP;; Cha-GAL80 females were crossed either to UAS-Dcr2 males (control 1 for possible effects of the UAS-Dcr2 construct alone) or to w^{1118} males (control 2 for the genetic background for the UAS-RNAi fly lines). The w^- mutation on the X-chromosome of w^{1118} is of no concern because it is not inherited by the experimental male progeny (which carries a wild-type white gene on X).

Intracellular Staining, Immunocytochemistry, and Image Acquisition. Adult flies were dissected to dye fill identified motoneurons with sharp electrodes and processed as described previously (19). We used anti Bruchpilot (29), Brp (nc82; DSHB, IA) to label Brp protein localized to presynaptic active zones,

as described previously (41). Stacks of optical sections with 0.3-μm thickness and 1,024 × 1,024-pixel resolution were acquired using a Leica TCS SP8 confocal laser scanning microscope with a 40× oil-immersion, 1.2 numerical aperture lens.

Electrophysiology. In situ patch clamp recordings of identified motoneurons were conducted as previously described (22, 23). Giant fiber (GF) stimulation and extracellular tungsten electrode recordings from identified wing depressor muscle fibers were conducted as previously described (43). MN5 firing activity was recorded in vivo during restrained flight with a sharpened tungsten electrode (diameter 100 μm) from the DLM flight muscle. Spike time precision error was defined as the percentage deviation from identical interspike time intervals during tonic firing. Expected time points for each MN5 spike were calculated from the average MN5 firing frequency. For each recorded spike the time difference from this expected time point was measured, averaged over all spikes of the bout, and normalized to the average expected spike time interval. Four parameters were measured after GF stimulation. Latency was measured as the average duration from 10 animals in each group between GF stimulation artifact and onset of DLM response (Fig. 1*H*). Refractory period is the minimal duration between two subsequent GF stimulations that result in two subsequent DLM fiber responses. The interval between GF stimuli was decreased in 0.1-ms increments starting with 6 ms. Experiments were repeated in 10 animals for each experimental group and averaged. Following frequencies is defined as the maximum frequencies at which all GF stimuli of a 10-stimuli bout result in muscle response (Fig. 1*K*). Following frequency 50% is defined as the frequency at which 50% of all GF stimuli result in a muscle response. Both were determined by increasing stimulation frequency from 100 Hz in 10-Hz increments.

Behavioral Testing. Tethered flight experiments were conducted as previously reported (28). Courtship song was recorded with a custom-built microphone, and sound tracks were digitized with a Digidata 1320A and analyzed with pClamp10.4 (Molecular Devices) and Spike 2 software (Cambridge Electronic Design). For courtship song recordings and analysis of mating success, single pairs of previously isolated 2-d-old virgin female and virgin male flies were placed into a Plexiglas chamber of 1-cm diameter and 3-mm height that was placed directly on top of the microphone. For phototaxis flies were given 20 s to choose to enter either an illuminated or a dark tube (1 cm in diameter) at a T-joint. Flies were assessed in two trials separated by 10 min of rest. Performance was calculated as the percentage of flies collected from the illuminated arm (Fig. 1*I*). For geotaxis, five male flies were transferred into a plastic tube (1-cm diameter, 12-cm length). After a 1-min acclimation period, flies were tapped to the ground to then record the number of flies that climbed beyond the 8-cm mark within 10 s. Flies were assessed in 10 consecutive trials separated by 15 s of rest. Performance is the percentage of flies passing the 8-cm mark averaged over 10 sessions (10 groups of five flies per genotype).

Statistical Analysis. All statistical analysis was conducted with SPSS 22 (IBM). Kruskal-Wallis ANOVA was used for nonparametric data and Mann-Whitney *U* test for between-group post hoc comparisons. For parametric data ANOVA with Newman Keuls and Scheffé post hoc comparisons was used. Statistical significance was defined as $^{**}P < 0.01$; $^{*}P < 0.05$.

ACKNOWLEDGMENTS. This study was supported by National Institutes of Health Grant 1RO1NS072128 and by German Research Foundation Grant Du 331/6-1 (to C.D.).

1. Fiala JC, Spacek J, Harris KM (2008) Dendritic structure. *Dendrites*, eds Stuart G, Sprouston N, Häusser M (Oxford University Press, New York), pp 1–34.
2. Azevedo FA, et al. (2009) Equal numbers of neuronal and nonneuronal cells make the human brain an isometrically scaled-up primate brain. *J Comp Neurol* 513(5):532–541.
3. Purves D, Hume RI (1981) The relation of postsynaptic geometry to the number of presynaptic axons that innervate autonomic ganglion cells. *J Neurosci* 1(5):441–452.
4. Gabbiani F, Krapp HG, Koch C, Laurent G (2002) Multiplicative computation in a visual neuron sensitive to looming. *Nature* 420(6913):320–324.
5. Single S, Borst A (1998) Dendritic integration and its role in computing image velocity. *Science* 281(5384):1848–1850.
6. Branco T, Häusser M (2010) The single dendritic branch as a fundamental functional unit in the nervous system. *Curr Opin Neurobiol* 20(4):494–502.
7. Ludwig M, Pittman QJ (2003) Talking back: Dendritic neurotransmitter release. *Trends Neurosci* 26(5):255–261.
8. Magee JC (2000) Dendritic integration of excitatory synaptic input. *Nat Rev Neurosci* 1(3):181–190.
9. London M, Häusser M (2005) Dendritic computation. *Annu Rev Neurosci* 28:503–532.
10. Koch C, Segev I (2000) The role of single neurons in information processing. *Nat Neurosci* 3(Suppl):1171–1177.
11. Kaufmann WE, Moser HW (2000) Dendritic anomalies in disorders associated with mental retardation. *Cereb Cortex* 10(10):981–991.
12. Kulkarni VA, Firestein BL (2012) The dendritic tree and brain disorders. *Mol Cell Neurosci* 50(1):10–20.
13. Vonhoff F, Duch C (2010) Tiling among stereotyped dendritic branches in an identified *Drosophila* motoneuron. *J Comp Neurol* 518(12):2169–2185.
14. Levine JD, Wyman RJ (1973) Neurophysiology of flight in wild-type and a mutant *Drosophila*. *Proc Natl Acad Sci USA* 70(4):1050–1054.
15. Ewing A (1977) The neuromuscular basis of courtship song in *Drosophila*: The role of indirect flight muscles. *J Comp Physiol A Neuroethol Sens Neural Behav Physiol* 119: 249–265.
16. Yamamoto D, Koganezawa M (2013) Genes and circuits of courtship behaviour in *Drosophila* males. *Nat Rev Neurosci* 14(10):681–692.
17. Ikeda K, Koenig JH (1988) Morphological identification of the motor neurons innervating the dorsal longitudinal flight muscle of *Drosophila melanogaster*. *J Comp Neurol* 273(3):436–444.
18. Koenig JH, Ikeda K (1980) Neural interactions controlling timing of flight muscle activity in *Drosophila*. *J Exp Biol* 87:121–136.
19. Duch C, Vonhoff F, Ryglewski S (2008) Dendrite elongation and dendritic branching are affected separately by different forms of intrinsic motoneuron excitability. *J Neurophysiol* 100(5):2525–2536.
20. Vonhoff F, Kuehn C, Blumenstock S, Sanyal S, Duch C (2013) Temporal coherency between receptor expression, neural activity and AP-1-dependent transcription regulates *Drosophila* motoneuron dendrite development. *Development* 140(3):606–616.
21. Kuehn C, Duch C (2013) Putative excitatory and putative inhibitory inputs are localised in different dendritic domains in a *Drosophila* flight motoneuron. *Eur J Neurosci* 37(6):860–875.
22. Ryglewski S, Duch C (2009) Shaker and Shal mediate transient calcium-independent potassium current in a *Drosophila* flight motoneuron. *J Neurophysiol* 102(6):3673–3688.
23. Ryglewski S, Lance K, Levine RB, Duch C (2012) Ca(v)2 channels mediate low and high voltage-activated calcium currents in *Drosophila* motoneurons. *J Physiol* 590(Pt 4): 809–825.
24. Consoulas C, Restifo LL, Levine RB (2002) Dendritic remodeling and growth of motoneurons during metamorphosis of *Drosophila melanogaster*. *J Neurosci* 22(12): 4906–4917.
25. Ryglewski S, Kilo L, Duch C (2014) Sequential acquisition of cacophony calcium currents, sodium channels and voltage-dependent potassium currents affects spike shape and dendrite growth during postembryonic maturation of an identified *Drosophila* motoneuron. *Eur J Neurosci* 39(10):1572–1585.
26. Hutchinson KM, Vonhoff F, Duch C (2014) Dscam1 is required for normal dendrite growth and branching but not for dendritic spacing in *Drosophila* motoneurons. *J Neurosci* 34(5):1924–1931.
27. Allen MJ, Godenschwege TA, Tanouye MA, Phelan P (2006) Making an escape: Development and function of the *Drosophila* giant fibre system. *Semin Cell Dev Biol* 17(1):31–41.
28. Brembs B, Christiansen F, Pflüger HJ, Duch C (2007) Flight initiation and maintenance deficits in flies with genetically altered biogenic amine levels. *J Neurosci* 27(41): 11122–11131.
29. Kittel RJ, et al. (2006) Bruchpilot promotes active zone assembly, Ca2+ channel clustering, and vesicle release. *Science* 312(5776):1051–1054.
30. Fayyazuddin A, Zaheer MA, Hiesinger PR, Bellen HJ (2006) The nicotinic acetylcholine receptor Dalpha7 is required for an escape behavior in *Drosophila*. *PLoS Biol* 4(3):e63.
31. Fuerst PG, et al. (2009) DSCAM and DSCAML1 function in self-avoidance in multiple cell types in the developing mouse retina. *Neuron* 64(4):484–497.
32. Machin KE, Pringle JWS (1959) The physiology of insect fibrillar muscle. II. Mechanical properties of a beetle flight muscle. *Proc R Soc B* 151:204–225.
33. Dickinson MH, Tu MS (1997) The function of dipteran flight muscle. *Comp Biochem Physiol A* 116(3):223–228.
34. Gordon S, Dickinson MH (2006) Role of calcium in the regulation of mechanical power in insect flight. *Proc Natl Acad Sci USA* 103(11):4311–4315.
35. Shirangi TR, Stern DL, Truman JW (2013) Motor control of *Drosophila* courtship song. *Cell Reports* 5(3):678–686.
36. Coen P, et al. (2014) Dynamic sensory cues shape song structure in *Drosophila*. *Nature* 507(7491):233–237.
37. Zwart MF, Randlett O, Evers JF, Landgraf M (2013) Dendritic growth gated by a steroid hormone receptor underlies increases in activity in the developing *Drosophila* locomotor system. *Proc Natl Acad Sci USA* 110(40):E3878–E3887.
38. Dierssen M, Ramakers GJ (2006) Dendritic pathology in mental retardation: From molecular genetics to neurobiology. *Genes Brain Behav* 5(Suppl 2):48–60.
39. Meunier C, Segev I (2002) Playing the devil's advocate: Is the Hodgkin-Huxley model useful? *Trends Neurosci* 25(11):558–563.
40. Brand AH, Perrimon N (1993) Targeted gene expression as a means of altering cell fates and generating dominant phenotypes. *Development* 118(2):401–415.
41. Boerner J, Duch C (2010) Average shape standard atlas for the adult *Drosophila* ventral nerve cord. *J Comp Neurol* 518(13):2437–2455.
42. Dietzl G, et al. (2007) A genome-wide transgenic RNAi library for conditional gene inactivation in *Drosophila*. *Nature* 448(7150):151–156.
43. Kadas D, Tzortzopoulos A, Skoulakis EM, Consoulas C (2012) Constitutive activation of Ca2+/calmodulin-dependent protein kinase II during development impairs central cholinergic transmission in a circuit underlying escape behavior in *Drosophila*. *J Neurosci* 32(1):170–182.